

Molecular dynamics study of surface-tethered $S(\text{CH}_2\text{CH}_2\text{O})_6\text{CH}_3$: Helix formation and thermal disorder

R.D. Mountain^a, V. Simmons^b, C.W. Meuse^{c,*}, J.B. Hubbard^d

^a Physical and Chemical Properties Division, National Institute of Standards and Technology, 100 Bureau Dr, Gaithersburg, MD 20899, USA

^b 1337 Cordova Rd, Pittsburgh, PA 15206, USA

^c Biochemical Science Division, National Institute of Standards and Technology, 100 Bureau Dr, Gaithersburg, MD 20899, USA

^d 51 Oak Shade Rd, Gaithersburg, MD 20878, USA

ARTICLE INFO

Article history:

Received 3 July 2008

Accepted 31 July 2008

Available online 11 September 2008

Keywords:

Molecular dynamics

Ethylene oxide

Monolayer

Helix

Thermal disorder

Surface tethered

Cavities

Voids

ABSTRACT

We present the results of a molecular dynamics study of a set of surface-tethered $S(\text{CH}_2\text{CH}_2\text{O})_6\text{CH}_3$ chains. In this study, we analyze helix formation, in addition to thermal disorder, and find that spontaneous helix formation and details of helix morphology depend on charge partitioning ascribed to oxygen and the methylene groups. The effects of varying surface coverage as well as chain–surface interaction strength indicate that a set of approximately $\frac{7}{2}$ helical structures oriented predominantly normal to the surface are formed at near full coverage. This occurs even though thermal disorder clearly precludes a description based on the concept of a perfect crystalline monolayer. Thermal fluctuations in chain morphology in the vicinity of the terminal methyl groups lead to the exposure of oxygen to the external environment. We also find that the persistence of compact helix-containing domains at partial surface coverage results in the formation of well-defined cavities or void regions that expose the bare surface, even in the presence of strong chain–surface attractive interactions.

Published by Elsevier Inc.

1. Introduction

We employ molecular dynamics (MD) simulation to qualitatively explore and quantify structural features of self-assembled monolayers of surface tethered polyethylene oxide (PEO) chains. The detailed morphology of composite, surface-grafted, PEO-containing monolayers is currently believed to play an important role in conferring resistance of the surface to non-specific protein adsorption [1–12]. While these systems have been the subject of a number of intensive experimental and theoretical investigations, there remain unresolved issues that may be at least partially addressed by the judicious use of MD. For example, the dependence of chain ordering on atomic and surface interaction potentials can be studied in the presence of statistical and thermal fluctuations. Microscopic structural features, not readily accessible to experimental probes, can then be examined under a variety of physical conditions. In particular, we investigate the helical structures formed from a monolayer of $S(\text{EO})_6\text{CH}_3$, where $\text{EO} = -\text{CH}_2\text{CH}_2\text{O}-$.

There exists infrared spectroscopic evidence that this monolayer consists of $\frac{7}{2}$ helices oriented normal to the (gold) tethering surface [7,12], and so we attempt to construct a “minimal model” interaction potential, based on a model for *amorphous* polyethy-

lene oxide, which results in a good approximation to this particular morphology. Our choice of an amorphous model for PEO, rather than a crystalline model, is motivated by the desire to answer the question, “To what extent do surface and intermolecular interactions play a role in the spontaneous formation of positional, orientational, and helical order in these systems?” Our simulations indicate that we are reasonably successful if the nearest neighbor O–O separation distance is chosen as the principal criterion of a $\frac{7}{2}$ -like helical order. We find that, even in the presence of thermal disorder, our simulation results are not inconsistent with structural rationalizations from observed IR adsorption bands that are based on models of ideal 2D polymer crystals.

The model employed in the simulation is described in Section 2. This section also contains a description of the simulations and introduces various measures used to characterize the structure of the monolayers.

2. Model and simulation details

A united atom representation of a 20-site $S(\text{EO})_6\text{CH}_3$ molecule is employed in the following simulation (see Fig. 1). From a dynamical point of view this united atom simplification is justified because the first vibrational level for C–H stretch, H–C–H and H–C–C bend levels lie far in energy above that associated with the temperature (290 K) of these simulations. Although the bend modes are in the 1000 cm^{-1} to 1400 cm^{-1} range, these energies

* Corresponding author.

E-mail address: curtis.meuse@nist.gov (C.W. Meuse).

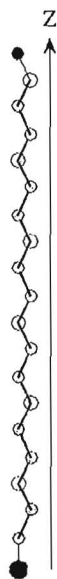


Fig. 1. Single surface-tethered $S(\text{EO})_6\text{CH}_3$ molecule consisting of 20 sites in an all trans configuration, with the S- CH_3 vector oriented normal to the surface. The large filled circle represents the thiol head group, the small filled circles represent the 12 united atom methylene units, the 6 oxygen atoms appear as large empty circles, and the united atom terminal methyl group is represented by a small filled circle.

correspond to a temperature 5-times the temperature of the system examined here, and may safely be excluded. From a structural point of view, the asphericity of the methylene and methyl groups and the modest degree of C-H charge separation are not expected to play major roles in overall chain morphology. The intra- and intermolecular parameters in this study are identical, unless otherwise noted, to those used by Lin et al. [13] in their MD simulation of amorphous, polydisperse polyethylene oxide, except that S in our model is generally treated as distinct from O. The total potential energy of the system, U , consists of the sum of a bonded term, a non-bonded term, and a surface interaction:

$$U = U_b + U_{nb} + U_{sur}. \quad (1)$$

The intramolecular bonded interactions consist of summations over the stretch, bend, and torsion modes; they extend to sets of nearest neighbor pairs for stretch, next nearest neighbors (triples) for bend, and next-next nearest neighbors (quadruples) for torsion:

$$U_b = \sum \frac{1}{2} K_r (\Delta r_i)^2 + \frac{1}{2} K_\theta (\Delta \theta_i)^2 + \frac{1}{2} U_2 (1 - \cos 2\phi_i) + \frac{1}{2} U_3 (1 + \cos 3\phi_i). \quad (2)$$

Here $\Delta r = (r - r_D)$, where D stands for the SC, CC, and CO equilibrium bond separations, and $\Delta \theta = (\theta - \theta_E)$, where E is the SCC, CCO, and COC equilibrium bend angles. ϕ is a torsion angle; i.e., the dihedral angle between the two planes formed by four adjacent sites associated with the quadruples SCCO, CCOC, and OCCO. The parameters for stretch, bend, and torsion are given in Table 1. For bonded interactions CH_2 is assumed to be identical to CH_3 .

The first non-bonded contribution to the potential energy, U_{lj} , is a Lennard-Jones interaction which acts between sites on the same molecule which are separated by three or more sites, as well as between a given site and those sites associated with all other molecules in the system. In this case CH_2 is distinct from CH_3 . The second term, U_q , is a direct electrostatic interaction between all pairs of partially charged sites in the system. This charge partitioning is assumed to occur only between the oxygen and methylene units (18 charged sites per molecule). We employ the same charge assignment as proposed for amorphous polyethylene oxide, which

Table 1
Stretch, bend, and torsion parameters.

Stretch	S-C	C-C	O-C
K_r (kJ/(mol Å ²))	2470	2470	2813
r_0 (Å)	1.538	1.538	1.423
Bend	S-C-C	C-C-O	C-O-C
K_θ (kJ/(mol rad ²))	523	523	469
θ_0	114.0	109.0	111.9
Torsion	S-C-C-O	C-C-O-C	O-C-C-O
U_2 (kJ/mol)	-2.106	0	-2.106
U_3 (kJ/mol)	12.04	12.04	12.04

Table 2
Lennard-Jones parameters^a and charge partitioning^b.

Sites	ϵ (kJ/mol)	σ (Å)
S-S	1.6620	4.582
CH_2 - CH_2	0.5044	3.425
CH_3 - CH_3	0.6283	4.038
O-O	0.3977	2.851
$q(\text{O}) = -0.326 e $		
$q(\text{CH}_2) = 0.163 e $		

^a Unlike site interaction parameters ϵ are determined from the geometric mean of like site parameters ($\epsilon_{ij} = (\epsilon_i \epsilon_j)^{1/2}$). Unlike site interaction parameters σ are determined from the arithmetic mean of like site parameters ($\sigma_{ij} = \frac{1}{2}(\sigma_i + \sigma_j)$).

^b e has units of electron charge.

was determined from experimental data on the dipole moment and equilibrium configuration of the dimethyl ether molecule [13]. The Lennard-Jones parameters and partial charge assignments are given in Table 2. The non-bonded contribution to U , U_{nb} , takes the form

$$U_{nb} = U_{lj} + U_q, \quad (3)$$

$$U_{lj} = \sum_{\text{sites}} \left[\left(\frac{\sigma}{r} \right)^{12} - \left(\frac{\sigma}{r} \right)^6 \right], \quad (4)$$

$$U_q = \sum_{\text{sites}} \frac{q_i q_j}{|r_i - r_j|}. \quad (5)$$

All non-bonded interactions are assumed to terminate at a distance of 1.2 nm; long range dispersion interactions and electrostatic effects are not included in our model (no long-range corrections were applied).

Finally, since the 9-3 potential usually used in simulations of this type has been found not to accurately fit the binding energy, distance from the surface, and dispersion coefficient, the surface interaction term takes the form developed by Hautman and Klein [14]. The surface we are trying to model in this case is Au(111) and has the form

$$U_{sur} = \frac{A}{(z - z_0)^{12}} - \frac{B}{(z - z_0)^3}. \quad (6)$$

The strong repulsion at short distances ensures an impenetrable surface, due to the $(z - z_0)^{12}$ term, whereas the attractive portion, due to the $(z - z_0)^3$ term, serves to firmly tether S while influencing the overall structure of the chains. The surface interaction parameters are given in Table 3. Note that the B parameter for S is larger by a factor of ≈ 100 compared to B for the other groups. In summary, our interaction potential is based on a model for amorphous polyethylene oxide, supplemented by a chain-surface interaction and strong S-surface tethering.

Our simulations cell contains 225 $S(\text{EO})_6\text{CH}_3$ molecules tethered via a strong short range S-surface interaction. The overall chain-surface potential is translation-invariant with respect to directions parallel to the surface, so that lateral motion is inhibited only by the presence of nearby molecules. The chains are located in an $L \times L$ square planar region subject to periodic boundary con-

Table 3
Parameters for the surface interactions.

Sites	A (kJ/(mol Å ¹²))	B^a (kJ/(mol Å ³))	z_0 (Å)
S	283,224	1501	0.269
CH ₂	232,741	14.21	0.860
CH ₃	260,997	17.28	0.860
O	264,345	17.44	0.860

^a The weak surface interaction case is obtained by dividing B by 10 for CH₂, CH₃, and O.

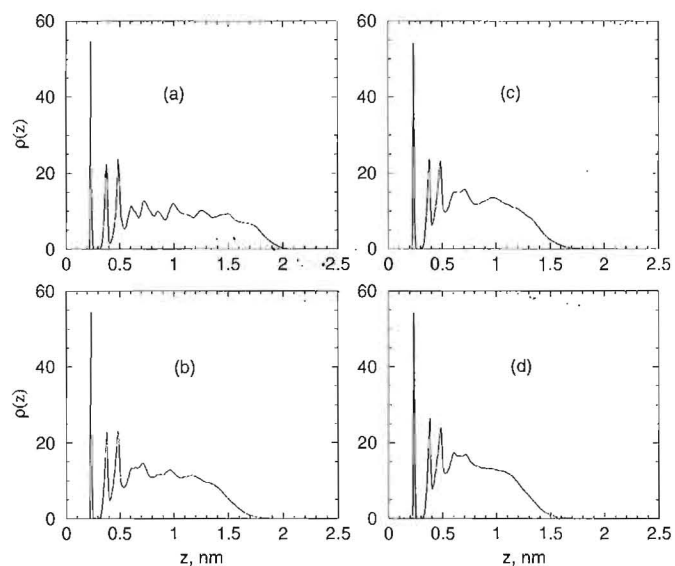


Fig. 2. From $z = 0$ the Au surface, we plot density profiles for four degrees of surface coverage: (a) full coverage at 0.214 nm^2 projected surface area per molecule, (b) $\frac{3}{4}$ full coverage, (c) $\frac{2}{3}$ full coverage, and (d) $\frac{1}{2}$ full coverage. The chain-surface interaction is weak and since the strong surface interaction causes similar behavior, it is not displayed.

ditions in the lateral direction. The z -axis is chosen normal to the surface which is located in the $z = 0$ plane. The cell dimension, L , is adjusted so that the surface area available per chain varies by steps from that corresponding to a close-packed density of 0.214 nm^2 , inferred from measurements on monolayers adsorbed onto Au, to twice this value. The simulations were initiated by placing the chains in a vertical orientation with respect to the tethering surface in a perfect square-planar array. The starting configuration of each chain was taken as the all-trans conformation as depicted in Fig. 1. The thiol sites were set at 0.24 nm above the $z = 0$ plane, and the system was then allowed to evolve, subject to a Nosé-Hoover thermostat [15] that maintained the temperature at 290 K (NVT-ensemble). The classical mechanics equations of motion were integrated using the Beeman algorithm [16,17] with a time step of 1 fs to guarantee adequate resolution of the C-C and C-O stretching motions. The system was allowed to evolve until certain statistical measures of order, such as the density and orientation profiles, were invariant with respect to any further increases in simulation time, which was typically in the range of $100\text{--}200 \text{ ps}$. The attraction of the surface for the oxygen, methyl, and methylene groups was chosen as *weak* and are shown in Table 3. Since the two sets of simulations, corresponding to strong and weak surface interactions, yielded nearly identical results for the various averages studied, the figures refer, with one exception, to the weak field case.

3. Simulation results

Three types of order are considered. The first is a collective atomic-level density profile of the chains relative to the tethering

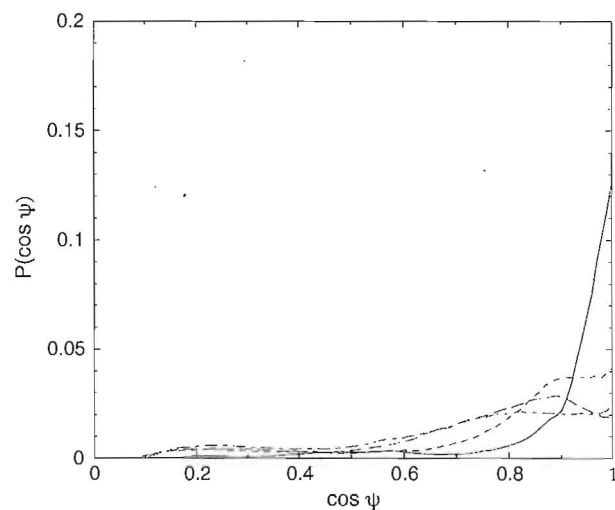


Fig. 3. The weak surface-interaction S-CH₃ tilt angle distributions. They are presented as the cosine of the angle that this vector makes with the surface normal vector and are shown for full surface coverage (solid line), $\frac{3}{4}$ full coverage (dashed line), $\frac{2}{3}$ full coverage (long dashed line), and $\frac{1}{2}$ full coverage (long-short dashed line). Results for the strong surface interaction are very similar and are not displayed.

surface (Fig. 2). The second measure of order is the distribution of S-CH₃ tilt angles relative to the surface normal (Fig. 3). The third measure of order consists of the distribution of various O-O intramolecular separation distances (Figs. 4 and 5). This function provides a succinct statistical description of helix morphology at several length scales which is compared with ideal helical order. These quantitative measures of order are then supplemented by instantaneous projected images of the collection of chains that provide a qualitative but informative picture of the behavior of the entire surface array (Figs. 6–10).

The number density profiles (Fig. 2) consist of plots of the number of united atom sites located in bins of width dz away from the surface. The orientation distributions (Fig. 3) are plots of the cosines of the tilt angle of the S-CH₃ unit vector relative to the surface normal. The cosines of these tilt angles are binned with a resolution of 0.01 degrees. The orientation distribution can be interpreted as the fractional density of chains having a prescribed projection onto the z -axis. The third measure of order, the intramolecular separation, is intended to quantify the notion of helicity. This consists of calculating the average nearest neighbor (NN), 2nd NN, etc., set of oxygen-oxygen (O-O) Euclidean distances (not z -projected distances) for each chain, with a resolution of 0.00316 nm , and then averaging over all molecules in the system. This has the effect of measuring average helix order relative to each individual molecular frame as opposed to a surface or lab-fixed frame. The z -projected number density profiles for various degrees of surface coverage are shown in Fig. 2.

The united atom representation implies that S, CH₂ and O, and CH₃ all have the same statistical weight. At the close-packed density, the maximum of the S peak lies at 0.237 nm above the surface where $z = 0$; the second peak, assigned to CH₂, is centered at 0.368 nm , and the third, which most likely consists of nearly co-planar CH₂ and O, resides at 0.465 nm . Beyond this point the profile, blurred by fluctuations, eventually terminates at around 2.02 nm from the surface, which is in accord with the S(E₀)₆CH₃ monolayer on gold thickness inferred from recent spectroscopic ellipsometric measurements [12]. At reduced surface densities these distributions lose their outer structural features and become more compressed toward $z = 0$; at $\frac{1}{2}$ full coverage the profile termination distance (maximum chain extension) has diminished to 1.61 nm .

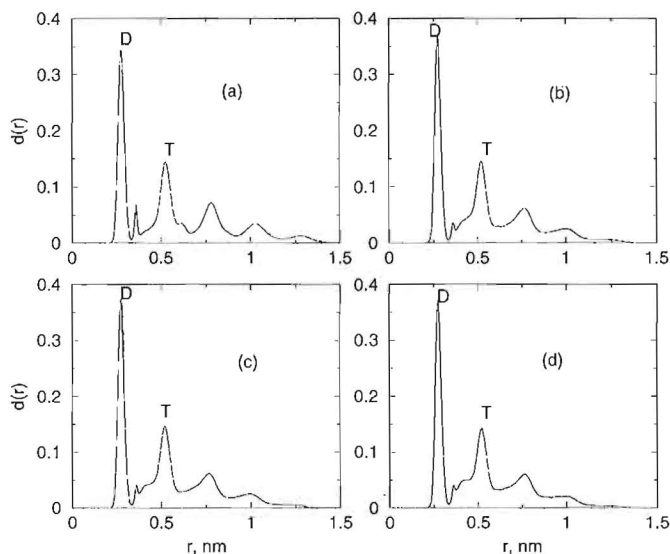


Fig. 4. Distributions of intramolecular O–O separation distances for weak chain–surface interaction are shown for four degrees of surface coverage: (a) full coverage, (b) $\frac{3}{4}$ full coverage, (c) $\frac{2}{3}$ full coverage, and (d) $\frac{1}{2}$ full coverage. Similar results for the strong surface interaction are not displayed. Maxima of the nearest neighbor O–O distance (diads) are labeled D and maxima of the next nearest neighbor O–O distance (triads) are labeled T.

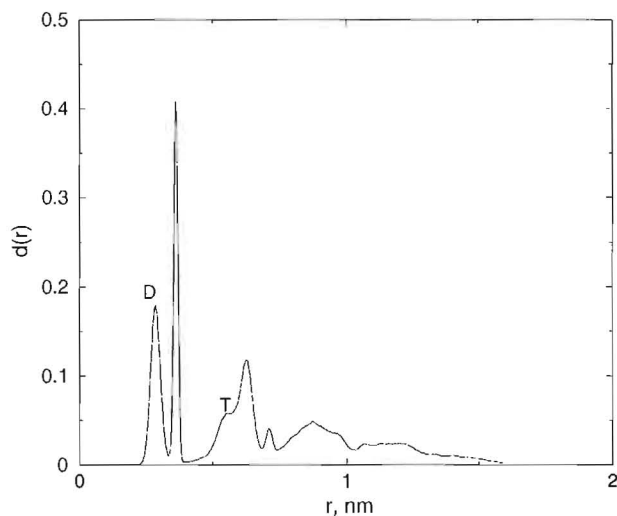


Fig. 5. The distribution of intramolecular O–O separation distances in the absence of any electrostatic interactions is shown for the full surface coverage case. The nearest neighbor O–O distance (diads) are labeled D and the next nearest neighbor O–O distance (triads) are labeled T.

At full coverage the chain orientation, shown in Fig. 3, is decidedly normal to the surface with a modest though non-negligible dispersion of roughly 7° . At $\frac{3}{4}$ full coverage a secondary component is evident, located at about 75° from upright, while the maximum has shifted away from upright by about 20° . Note the factor of ≈ 3 reduction in the maximum orientation amplitude relative to the full coverage case. At $\frac{2}{3}$ full coverage the orientation distribution has become weakly bimodal, with the maximum now shifted by $\approx 30^\circ$ from the normal. At $\frac{1}{2}$ full coverage the maximum amplitude has shrunk considerably relative to the previous case, the overall distribution has broadened, and the secondary component has become more prominent.

The distributions of NN, 2nd NN, etc., intramolecular O–O separation distances are shown in Fig. 4. At full coverage the NN O–O maximum (diad, D) is located at 0.277 nm. We also find a small though distinct satellite peak at 0.365 nm which suggests a trans

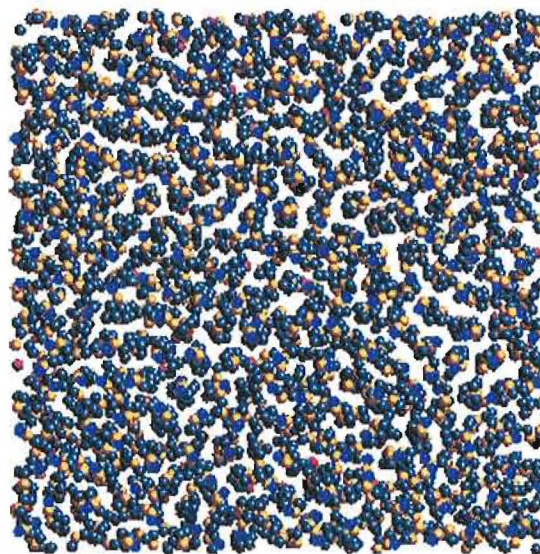


Fig. 6. The projected snapshot view of all 225 chains as viewed from a vertical position located above the terminal methyl groups; this picture was taken at full surface coverage. The small dark blue spheres represent the terminal methyl groups, large yellow spheres are oxygen, small grey spheres are methylenes, and the small red spheres are sulfur. Even though the chains are predominately in an upright position and the lateral pattern is roughly hexagonal, a considerable departure from the notion of perfect crystalline ordering (due to thermal fluctuations) is evident.

conformation, a 2nd NN O–O maximum (triad, T) at 0.528 nm, and a third located at around 0.79 nm. An ideal $\frac{7}{2}$ helix morphology gives 0.297 nm and 0.577 nm for the NN and 2nd NN O–O separations [18,19], which implies that the simulation result is consistent with this structure at short distances, but that discrepancies arise for larger O–O separations. Incidentally, the ratio of NN to 2nd NN peak locations, $0.277/0.528 = 0.525$ and $0.297/0.577 = 0.515$, respectively, differs by only 2% for simulation vs $\frac{7}{2}$ helix. At lower surface coverage, the satellite peak is less distinct whereas the NN O–O peak becomes slightly sharper. Both the z-projected density profiles and the O–O separation distance distributions vary only slightly from full to $\frac{1}{2}$ full coverage, whereas the tilt angle distributions are much more sensitive to the degree of surface packing. This seems to be consistent with a picture of somewhat flexible but intact helical structures that tend to topple over at reduced coverage.

Fig. 5 presents an intramolecular O–O distance distribution obtained from a simulation in which there is no methylene–oxygen charge partitioning, so that electrostatic interactions are entirely absent. All other aspects of the simulation remain unchanged. In contrast to the previous results with charge separation there now appears a very sharp feature indicative of molecules in a trans conformation at 0.352 nm, along with a smaller helix-like NN O–O peak situated at 0.271 nm.

A series of snapshot views looking down on the surface-tethered array along the z-axis is presented in Fig. 6 through Fig. 10. The size of the connected balls forming the chains has been scaled down from what would be inferred from more realistic molecular models so as to provide contrast for the projected structure. The small dark blue spheres that represent the terminal methyl groups do not form a well-ordered hexagonal pattern; this is clearly inconsistent with the notion of a perfect lamellar crystal. Also, the prominence of some of the large yellow spheres representing oxygen indicates that these groups may be exposed to the external environment. A key feature revealed by this series of snapshots is the appearance, at close to $\frac{1}{2}$ full surface coverage, of well-defined cavities that expose the bare surface, an effect that persists even in the presence of strong chain–surface interactions. Experimental evidence for the existence of these cavities at

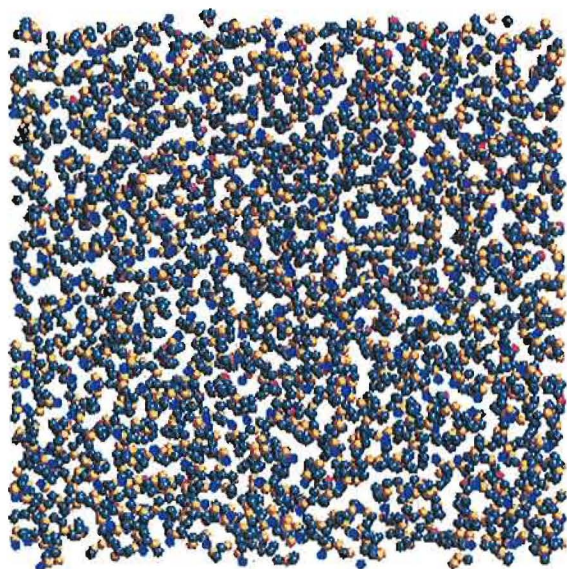


Fig. 7. Snapshot view of the chains at $\frac{3}{4}$ full surface coverage. There is a clear resemblance to the full coverage picture; however, a closer inspection reveals that a substantial fraction of the chains are tilted away from an upright position. This effect is clearly seen in the association orientation distribution in Fig. 3.

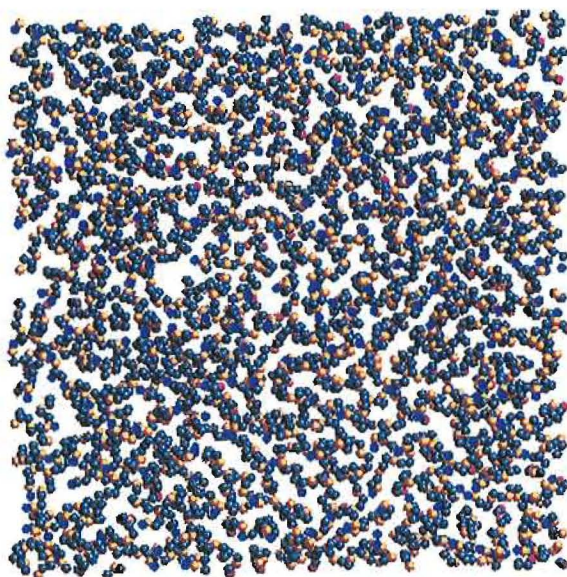


Fig. 8. Snapshot view of the chains at $\frac{2}{3}$ full surface coverage. There still is a clear resemblance to both the full coverage and the $\frac{3}{4}$ full coverage cases; however, the associated orientation distribution, in Fig. 3, now has a distinctly bimodal character.

these surface densities also exists as this range of densities preferentially adsorbs protein [20]. Insofar as the three measures of ordering considered here show no dramatic changes as the surface interaction is switched from *weak* to *strong*, we arrive at the picture of relatively robust domains of predominately upright helical molecules (at high surface coverage) with a considerable amount of thermal disorder.

Another principal finding of this study is the importance of intermolecular interactions, and in particular, partial charge-based electrostatic interactions, in spontaneous helix formation and morphology. In fact, we have performed Brownian dynamics simulations on a single tethered S(EO)₆CH₃ chain in vacuum which, under room temperature conditions, produces a disordered structure with an O–O distribution which is not in accord with what we observe in our MD simulation of 225 interacting molecules.

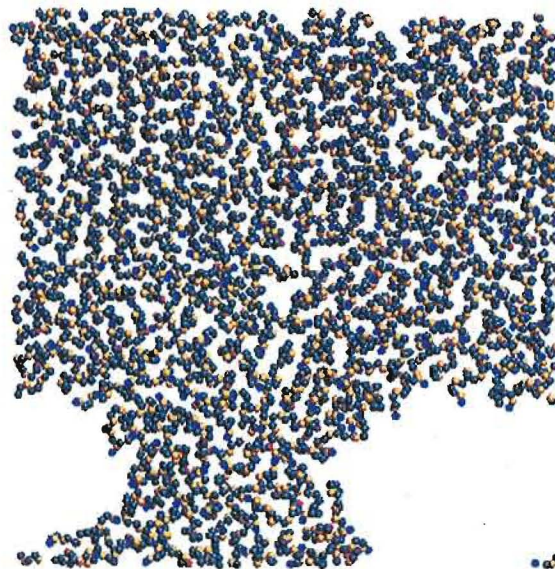


Fig. 9. Snapshot view of the chains at $\frac{1}{2}$ full surface coverage with a weak chain-surface interaction. There is a qualitative difference between this picture and those associated with higher coverage, insofar as well-defined cavities or regions completely devoid of chains are now apparent. The associated orientation distribution, in Fig. 3, still resembles that for the $\frac{2}{3}$ full coverage case. Cavities are not observed at $\frac{2}{3}$ full surface coverage, even after equilibration times of 200 ps, which suggests that they may begin to appear over a rather narrow range of surface densities. This has also been observed experimentally during protein adsorption [20].

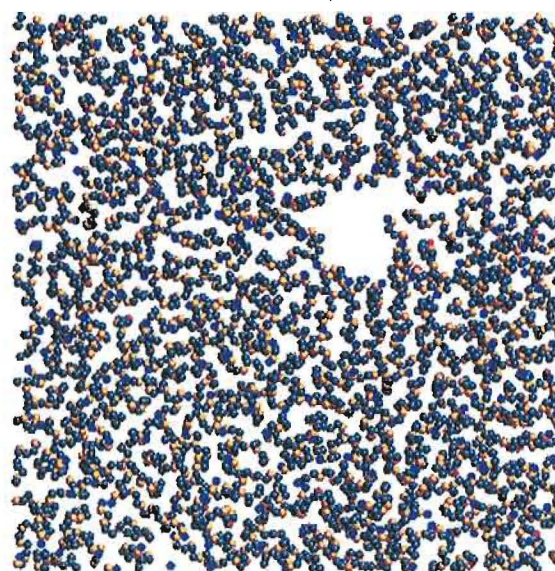


Fig. 10. Snapshot view of the chains at 0.54 full coverage with a strong chain-surface interaction; note the appearance of a small though well-defined cavity. As in the weak surface interaction case, for the strong surface interaction case, cavities are not observed at $\frac{2}{3}$ full coverage, although large cavities are apparent at $\frac{1}{2}$ full coverage. Experimental evidence also supports the existence of these cavities during the adsorption of protein [20].

The significance of partial charge assignments is suggested by the fact that, in the complete absence of charge separation, the O–O distance distribution shows a very prominent (NN) trans-like peak located at 0.352 nm. While an explicit representation of the methylene hydrogen atoms might be expected to have consequences for detailed helix morphology, we do not believe that this can serve as a major factor in helix formation in PEO chains. Furthermore, we found that helix morphology depends to some degree on the details of charge partitioning; in fact, excessive charge separation between oxygen and the methylenes resulted in collapse of the he-

lix morphology into a set of compact though disordered spiral-like structures.

4. Conclusion

We have investigated the types of order that spontaneously develop in surface-tethered PEO chain molecules as the coverage is varied from close-packed to $\frac{1}{2}$ of the close-packed density, and the strength of the interaction between the tethering surface and the methylene, oxygen, and terminal methyl groups of the chains is switched from *strong* to *weak*. We find that a rather simple model of amorphous PEO exhibits a rich variety of spontaneous ordering effects caused by surface interactions and packing; these include clustering, orientational ordering, and helix formation. In contrast to a previous MD study of surface-tethered octadecanethiol molecules, we find no tendency for $S(\text{EO})_6\text{CH}_3$ to collapse onto the surface as a disordered film at reduced surface coverage and strong chain-surface attraction [21,22]. Instead, the PEO chains remain oriented predominately normal to the surface with a structure that resembles a $\frac{7}{2}$ helix, thereby producing well-defined cavity regions which expose the bare surface along with oxygen atoms associated with domain wall chains. The different behaviors between the two systems could be due to the presence of charge partitioning in the PEO model and the absence of charge partitioning in the alkane chain model.

In addition, this study indicates that high resolution density profiles are poor indicators of average chain morphology, insofar as profile thermal broadening, associated mostly with backbone vibrational motion and bending, tends to obliterate structural features that are not located close to the tethering surface. Direct evidence for this backbone rocking is provided by the orientation distribution profiles of the $S-\text{CH}_3$ vector. In order to help clarify the situation a *helix order parameter distribution* is introduced which focuses on the density of various intramolecular O–O separations. This consists of constructing a plot of the fraction of the nearest, 2nd nearest, etc. distances between all pairs of oxygen atoms on each chain, and then averaging over all chains in the simulation. This function provides a compact measure of helix morphology and order which varies from local separations, corresponding to nearest neighbor O–O distances, to long-range separations, which corresponds to first-last O–O distances. Whereas the nearest neighbor peak at 0.277 nm accords reasonably well with the ideal $\frac{7}{2}$ helix value of 0.297 nm, we observe significant discrepancies at larger O–O separations. In particular, we find a satellite peak at a separation of 0.365 nm which is attributed to a distinct locally extended trans-like chain morphology and which accounts for 7% of the total nearest neighbor population. We conclude that surface-tethered $S(\text{EO})_6\text{CH}_3$, as modeled in our simulation, does resemble a $\frac{7}{2}$ helix

for short-range correlations, but that thermal fluctuations significantly disrupt long-range helical order.

The presence of considerable disorder away from the surface in the central and terminal portions of the chains is apparent from both the density profiles and $S-\text{CH}_3$ orientation distributions. Even at close packed density, the combination of backbone re-orientation and bond bending leads to considerable exposure of O in the terminal methoxy group, to the external environment. At first this pronounced disorder might seem incompatible with the infrared transition dipole-dipole coupling theory of Kobayashi and Sakashita [23] (KS), as these authors base their analysis on a perfect lamellar crystal structure. However, a unified dipole is assumed by KS to consist of 7 (PEO) chemical units (a unit cell), which is larger than an entire chain in our simulation. In addition, the lateral disorder associated with an imperfect hexagonal lattice, even when combined with orientation disorder in the transition dipoles, may have only a minor influence on the value of the so-called geometric factor, which consists of an orientationally weighted lattice sum and which plays a central role in the IR frequency shift predicted by KS.

References

- [1] P. Harder, M. Grunze, R. Dahint, G.M. Whitesides, P.E. Laibinis, *J. Phys. Chem. B* 102 (1998) 426.
- [2] A.J. Pertsin, M. Grunze, *Langmuir* 16 (2000) 8829.
- [3] H.J. Taunton, C. Toprakcioglu, L.J. Fetters, J. Klein, *Nature* 332 (1988) 712.
- [4] S.I. Jeon, J.D. Andrade, *J. Colloid Interface Sci.* 142 (1991).
- [5] S.I. Jeon, H. Lee, J.D. Andrade, P.G. De Gennes, *J. Colloid Interface Sci.* 142 (1991) 149.
- [6] R.L.C. Wang, H.J. Kreuzer, M. Grunze, *J. Phys. Chem. B* 101 (1997) 9767.
- [7] D.J. Vanderah, C.W. Meuse, V. Silin, A. Plant, *Langmuir* 14 (1998) 6916.
- [8] R. Valiokas, S. Svedhem, S.C.T. Svensson, B. Liedberg, *Langmuir* 15 (1999) 3390.
- [9] D.J. Vanderah, C.P. Pham, S.K. Springer, V. Silin, C.W. Meuse, *Langmuir* 16 (2000) 6527.
- [10] A.J. Pertsin, M. Grunze, I.A. Garbuzova, *J. Phys. Chem. B* 102 (1998) 4918.
- [11] D.J. Vanderah, G. Valincius, C.W. Meuse, *Langmuir* 18 (2002) 4674.
- [12] D.J. Vanderah, H. La, J. Arsenault, R.S. Gates, V. Silin, C.W. Meuse, *Langmuir* 19 (2003) 3752.
- [13] B. Lin, P.T. Boinske, J.W. Halley, *J. Chem. Phys.* 105 (1996) 1668.
- [14] J. Hautman, M.L. Klein, *J. Chem. Phys.* 91 (1989) 4994.
- [15] G.J. Martyna, M.L. Klein, M. Tuckerman, *J. Chem. Phys.* 97 (1992) 2635.
- [16] P. Schofield, *Comput. Phys. Commun.* 5 (1973) 17.
- [17] D. Beeman, *J. Comput. Phys.* 20 (1976) 130.
- [18] T. Miyazawa, K. Fukushima, Y. Ideguchi, *J. Chem. Phys.* 37 (1962) 2764.
- [19] Y. Takahashi, H. Tadokoro, *Macromolecules* 23 (1973) 672.
- [20] D.J. Vanderah, H. La, J. Naff, V. Silin, K.A. Rubinson, *J. Am. Chem. Soc.* 126 (2004) 13639.
- [21] R.D. Mountain, J.B. Hubbard, C.W. Meuse, V. Simmons, *J. Phys. Chem. B* 105 (2001) 9503.
- [22] R.D. Mountain, J.B. Hubbard, C.W. Meuse, V. Simmons, NISTIR 6481 (2000).
- [23] M. Kobayashi, M. Sakashita, *J. Chem. Phys.* 96 (1992) 748.

